

Hard-core Hall tube in superconducting circuits

Xin Guan(关欣), Gang Chen(陈刚), Jing Pan(潘婧), and Zhi-Guo Gui(桂志国)
Citation: Chin. Phys. B, 2022, 31 (**8**): 080302. DOI: 10.1088/1674-1056/ac633b
Journal homepage: http://cpb.iphy.ac.cn; http://iopscience.iop.org/cpb

What follows is a list of articles you may be interested in

Quantum simulation of lattice gauge theories on superconducting circuits: Quantum phase transition and quench dynamics

Zi-Yong Ge(葛自勇), Rui-Zhen Huang(黄瑞珍), Zi-Yang Meng(孟子杨), and Heng Fan(范桁)
Chin. Phys. B, 2022, 31 (**2**): 020304. DOI: 10.1088/1674-1056/ac380e

Quantum computation and simulation with superconducting qubits

Kaiyong He(何楷泳), Xiao Geng(耿霄), Rutian Huang(黄汝田), Jianshe Liu(刘建设), and Wei Chen(陈炜)
Chin. Phys. B, 2021, 30 (**8**): 080304. DOI: 10.1088/1674-1056/ac16cf

Universal quantum control based on parametric modulation in superconducting circuits

Dan-Yu Li(李丹宇), Ji Chu(储继), Wen Zheng(郑文), Dong Lan(兰栋), Jie Zhao(赵杰), Shao-Xiong Li(李邵雄), Xin-Sheng Tan(谭新生), and Yang Yu(于扬)
Chin. Phys. B, 2021, 30 (**7**): 070308. DOI: 10.1088/1674-1056/ac01c3

Speeding up transmissions of unknown quantum information along Ising-type quantum channels

W J Guo(郭伟杰), L F Wei(韦联福)
Chin. Phys. B, 2017, 26 (**1**): 010303. DOI: 10.1088/1674-1056/26/1/010303

Quantum communication via controlled holes in the statistical distribution of excitations in a nanoresonator coupled to a Cooper pair box

C. Valverde, A.T. Avelar, and B. Baseia
Chin. Phys. B, 2012, 21 (**3**): 030308. DOI: 10.1088/1674-1056/21/3/030308

Hard-core Hall tube in superconducting circuits

Xin Guan(关欣)[1,†], Gang Chen(陈刚)[2,3,4], Jing Pan(潘婧)[1], and Zhi-Guo Gui(桂志国)[1]

[1] *Department of Materials and Chemical Engineering, Taiyuan University, Taiyuan* 030032, *China*
[2] *State Key Laboratory of Quantum Optics and Quantum Optics Devices, Institute of Laser Spectroscopy, Shanxi University, Taiyuan* 030006, *China*
[3] *Collaborative Innovation Center of Extreme Optics, Shanxi University, Taiyuan* 030006, *China*
[4] *Collaborative Innovation Center of Light Manipulations and Applications, Shandong Normal University, Jinan* 250358, *China*

(Received 18 February 2022; revised manuscript received 16 March 2022; accepted manuscript online 1 April 2022)

The Hall tube as a minimum model to simulate the integer quantum Hall effect is essential for exploring topological physics, while it has not been constructed in the recent developing successfully experiments on superconducting circuits. In this work, we propose a feasible experiment scheme using three legs superconducting circuits with transmon qubits to realize a Hall tube. Then we first investigate its topological properties. Since the time–reversal, particle–hole, and chiral symmetries are all broken for the system, the Hall tube belongs to the A class of the Altland–Zirnbauer classification. We obtain the corresponding topological phase transition both numerically and analytically. Since the chirality is a key character of the quantum Hall effect, we secondly investigate the chiral physics in the Hall tube. We find the topological protected chiral edge currents and discuss its robustness. Finally, we give the possible experimental observations of the topological state and topological protected chiral edge currents.

Keywords: Hall tube, superconducting circuits, topological phase transition, chiral edge currents

PACS: 03.67.Ac, 73.43.–f, 85.25.Cp, 71.10.–w **DOI:** 10.1088/1674-1056/ac633b

1. Introduction

As the forefront of condensed matter physics, topological physics raised enormous attention in the past decades. Topological insulators[1–4] lie at an important position of the researches of topological state, which is beyond Landau symmetry breaking theory and is characterized by topological edge states and topological invariants. An fundamental effect in the topological insulator is the quantum Hall effect[5–9] which is induced by an external magnetic field in two-dimensional system. One of the essential models to investigate the quantum Hall physics is the Hofstader–Harper (H–H) Hamiltonian[10] which has been intensively studied both in theories and experiments.[11–14] In recent cold atom experiments, H–H Hamiltonian was demonstrated both in ladders[15,16] and cylinder[17] systems, dubbed Hall ribbons and Hall tube respectively. These two models were constructed in one dimensional optical lattice with fermion and another dimension was synthetic using the internal degrees of freedom of atoms. Chiral edge currents and topological phase are observed in Hall ribbons and tube respectively. Moreover, the topological insulator emerging in Hall tube breaks the time–reversal, particle–hole, and chiral symmetries simultaneously and is protected by an inversion symmetry, which is same as the integer quantum Hall state. Therefore, Hall tube is the simplest model without using parameter space to simulate the integer quantum Hall effects.

On the other hand, superconducting circuits as a platform with fine tunability, long coherent time and high-precision measurement[18,19] can be used for quantum computation,[20,21] quantum information,[22,23] and quantum simulation.[24–27] Especially, in recent experiments, the topological physics have been investigated in superconducting circuits. Some topological concepts have been studied in parameter[28–31] and phase[32,33] space of superconducting qubits and resonators respectively. Moreover topological magnon insulator[34] has been simulated in single superconducting qubit chain. However the Hall tube as a a minimum model to simulate the integer quantum Hall effects has not been investigated in superconducting circuits which is much easier to construct the tube geometric structure in real space compared with the other artificial systems.

In this paper we propose a scheme to realize the Hall tube with superconducting circuits and explore the topological phase transition in this model. Since the chirality is an essential character of the Hall effect, we investigate the chirality of the Hall tube. We find the topological protected chiral edge currents and discuss its robustness. Finally, we give a feasible experimental scheme to observe the topological state and topological protected chiral edge currents.

2. Hard-core Hall tube in superconducting circuits

Figure 1(a) shows our proposed three-leg superconducting circuits with transmon qubits to realize a hard-core Hall tube with an effective magnetic flux per plaquette. Along each leg, the transmon qubits are coupled with their nearest-

[†]Corresponding author. E-mail: guanxin810712@163.com

© 2022 Chinese Physical Society and IOP Publishing Ltd

neighbor sites, while they interact with each other between legs at the same unit cell. All couplers are capacitors. Moreover, there exist both nearest-neighbor and next-nearest-neighbor couplings between the transmon qubits which has been realized in experiments.[35,36] The corresponding Lagrangian is written as

$$\begin{aligned}\mathcal{L} =& \sum_{\nu,j}\left[\frac{C_{\nu j}}{2}\dot{\phi}_{\nu j}^2+E_{\nu j}^J\cos\left(\frac{\phi_{\nu j}}{\phi_0}\right)\right]\\&+\sum_{\nu,\langle i,j\rangle}\left[\frac{C_{\nu ij}}{2}\left(\dot{\phi}_{\nu i}-\dot{\phi}_{\nu j}\right)^2\right]\\&+\sum_{j}\left[\frac{C_{ABj}}{2}\left(\dot{\phi}_{Aj}-\dot{\phi}_{Bj}\right)^2+\frac{C_{BCj}}{2}\left(\dot{\phi}_{Bj}-\dot{\phi}_{Aj}\right)^2\right.\\&\left.+\frac{C_{CAj}}{2}\left(\dot{\phi}_{Cj}-\dot{\phi}_{Aj}\right)^2\right].\end{aligned}\tag{1}$$

Here, $C_{\nu j}$ and $E_{\nu j}^J$ are the effective capacitance and the Josephson energy of the transmon qubit at the j-th site on the ν-th ($\nu=A,B,C$) leg. $\{C_{\nu(j-1)j},C_{\nu j(j+1)}\}$ and $\{C_{ABj},C_{BCj},C_{CAj}\}$ are the capacitors to couple the transmon qubits at the j-th site on the ν-th leg with its nearest-neighbor sites along each leg and between the legs, respectively. $\phi_{\nu j}$ is the node flux expressed in unit of the reduced flux quantum $\phi_0=1/(2e)$. The symbol $\langle i,j\rangle$ denotes that the summation runs over all pairs of the nearest-neighbor sites along each leg. With the canonical coordinate $\hat{\phi}_{\nu j}$, the canonical momentum $\hat{q}_{\nu j}=\partial L/\partial\dot{\hat{\phi}}_{\nu j}$, *i.e.*,

$$\begin{aligned}\hat{q}_{\nu j} =& C_{\nu j}\dot{\hat{\phi}}_{\nu j}+\sum_{j\langle i\rangle}C_{\nu j}\left(\dot{\hat{\phi}}_{\nu j}-\dot{\hat{\phi}}_{\nu j\langle i\rangle}\right)\\&+\sum_{\nu\neq\nu'}C_{\nu\nu' j}\left(\dot{\hat{\phi}}_{\nu i}-\dot{\hat{\phi}}_{\nu' i}\right),\end{aligned}\tag{2}$$

where $j\langle i\rangle$ indicates the summation of the nearest-neighbor sites around the j-th site. Considering the experimental condition that $C_{\nu j}\gg\{C_{\nu(j-1)j},C_{\nu j(j+1)},C_{ABj},C_{BCj},C_{CAj}\}$, we have $\dot{\hat{\phi}}_{\nu j}\approx\hat{q}_{\nu j}/C_{\nu j}$. Applying the Legendre transformation, the corresponding Hamiltonian is given by

$$\hat{H}=\hat{H}_0+\hat{H}_{\rm IJ}+\hat{H}_{\rm R},\tag{3}$$

where

$$\hat{H}_0=\sum_{\nu,j}\left(\frac{\hat{q}_{\nu j}^2}{2\tilde{C}_{\nu j}}+\frac{\hat{\phi}_{\nu j}^2}{2L_{\nu j}^J}-\frac{E_{\nu j}^J}{24\hat{\phi}_0^4}\hat{\phi}_{\nu j}^4\right),\tag{4}$$

$$\hat{H}_{\rm IJ}=\sum_{\nu,\langle i,j\rangle}\frac{C_{\nu ij}}{C_{\nu i}C_{\nu j}}\hat{q}_{\nu i}\hat{q}_{\nu j},\tag{5}$$

$$\hat{H}_{\rm R}=\sum_{\nu\neq\nu',j}\frac{C_{\nu\nu' j}}{C_{\nu j}C_{\nu' j}}\hat{q}_{\nu i}\hat{q}_{\nu' i},\tag{6}$$

with $1/\tilde{C}_{\nu j}=(C_{\nu j}-C_{ABj}-C_{BCj}-C_{CAj}-C_{\nu(j-1)j}-C_{\nu j(j+1)})/C_{\nu j}^2$ and $1/L_{\nu j}^J=E_{\nu j}^J/\phi_0^2$.

By introducing bosonic annihilation and creation operators

$$\hat{a}_{\nu j}=\sqrt{\frac{\tilde{C}_{\nu j}\omega_{\nu j}^0}{2}}\hat{\phi}_{\nu j}+{\rm i}\sqrt{\frac{1}{2\tilde{C}_{\nu j}\omega_{\nu j}^0}}\hat{q}_{\nu j},\tag{7}$$

$$\hat{a}_{\nu j}^\dagger=\sqrt{\frac{\tilde{C}_{\nu j}\omega_{\nu j}^0}{2}}\hat{\phi}_{\nu j}-{\rm i}\sqrt{\frac{1}{2\tilde{C}_{\nu j}\omega_{\nu j}^0}}\hat{q}_{\nu j},\tag{8}$$

where $[\hat{a}_{\nu j},\hat{a}_{\nu',j'}^\dagger]=\delta_{\nu,\nu'}\delta_{j,j'}$ and $\omega_{\nu j}^0=\sqrt{8E_{\nu j}^CE_{\nu j}^J}$ with $E_{\nu j}^C=e^2/(2\tilde{C}_{\nu j})$, and then performing a rotating-wave approximation, the Hamiltonian (3) is quantized as

$$\hat{H}_0=\sum_{\nu,j}\omega_{\nu j}^0\hat{a}_{\nu j}^\dagger\hat{a}_{\nu j}+\frac{1}{2}V_{\nu j}\hat{n}_{\nu j}(\hat{n}_{\nu j}-1),\tag{9}$$

$$\hat{H}_{\rm IJ}=\sum_{\nu,j}g_{\nu j}\hat{a}_{\nu(j-1)}^\dagger\hat{a}_{\nu j}+{\rm H.c.},\tag{10}$$

$$\hat{H}_{\rm R}=\sum_{\nu\neq\nu',j}\tilde{g}_{\nu\nu' j}\hat{a}_{\nu j}^\dagger\hat{a}_{\nu' j}+{\rm H.c.},\tag{11}$$

where H.c. is the Hermitian conjugate, $\hat{n}_{\nu j}=\hat{a}_{\nu j}^\dagger\hat{a}_{\nu j}$ is the particle number operator, and

$$V_{\nu j}=-E_{\nu j}^C,\tag{12}$$

$$g_{\nu j}=\frac{C_{\nu(j-1)j}\sqrt{\omega_{\nu(j-1)}^0\omega_{\nu j}^0}}{2\sqrt{C_{\nu(j-1)}C_{\nu j}}},\tag{13}$$

$$\tilde{g}_{\nu\nu' j}=\frac{C_{\nu\nu' j}\sqrt{\omega_{\nu j}^0\omega_{\nu' j}^0}}{2\sqrt{C_{\nu j}C_{\nu' j}}}.\tag{14}$$

In Eqs. (12)–(14), $V_{\nu j}$ denotes the anharmonicity of each qubit, $g_{\nu j}$ is the coupling strength between the qubits at the j-th and $(j-1)$-th sites on the ν-th leg, and $\tilde{g}_{\nu\nu' j}$ is the coupling strength between the qubits at the j-th sites on the ν-th and ν'-th legs. For simplicity, we take $g_{\nu j}=\tilde{g}_{\nu\nu' j}=g_0$. Since the transmon qubits request $E_{\nu j}^C\ll E_{\nu j}^J$,[37] here we choose $E_{\nu j}^J/E_{\nu j}^C=50$ and then consider $\{C_{\nu(j-1)j},C_{\nu j(j+1)},C_{ABj},C_{BCj},C_{CAj}\}\approx0.5$ fF and $C_{\nu j}\approx100$ fF. Based on these parameters, we have $V_{\nu j}/(2\pi)\approx200$ MHz and $g_0/(2\pi)\approx10$ MHz, which lead to a condition that $V_{\nu j}\gg g_0$. In such a case, the qubit exhibits strong anharmonicity and only one boson can be excited for each transmon qubit, which leads to $V_{\nu j}\hat{n}_{\nu j}(\hat{n}_{\nu j}-1)/2\equiv0$, and $\hat{a}_{\nu j}^\dagger|0\rangle_{\nu j}=|1\rangle_{\nu j}$, $\hat{a}_{\nu j}^\dagger|1\rangle_{\nu j}=0$, $\hat{a}_{\nu j}|0\rangle_{\nu j}=0$, and $\hat{a}_{\nu j}|1\rangle_{\nu j}=|0\rangle_{\nu j}$. As a result, the Hamiltonian (3) becomes

$$\begin{aligned}\hat{H} =& \sum_{\nu,j}\omega_{\nu j}^0\hat{a}_{\nu j}^\dagger\hat{a}_{\nu j}+\sum_{\nu,j}\left(g_{\nu j}\hat{a}_{\nu(j-1)}^\dagger\hat{a}_{\nu j}+{\rm H.c.}\right)\\&+\sum_{\nu\neq\nu',j}\left(\tilde{g}_{\nu\nu' j}\hat{a}_{\nu j}^\dagger\hat{a}_{\nu' j}+{\rm H.c.}\right),\end{aligned}\tag{15}$$

with the revised commutation relation

$$\left[\hat{a}_{\nu j},\hat{a}_{\nu',j'}^\dagger\right]=(1-2\hat{n}_{\nu j})\delta_{\nu,\nu'}\delta_{j,j'}.\tag{16}$$

To further realize a synthetic Hall tube shown in Fig. 1(b), two alternating-current microwave drivings of each transmon qubit are taken into account. These microwave drivings can

be achieved experimentally by the flux-bias lines.[38–40] In this case, each qubit frequency is modulated independently as

$$\omega_{vj}(t) = \omega_{vj}^0 + \varepsilon_{vj}\sin(u_{vj}t+\varphi_{vj}) + \varepsilon'_{vj}\sin\left(u'_{vj}t+\varphi'_{vj}\right), \tag{17}$$

where ε_{vj} and ε'_{vj}, u_{vj} and u'_{vj}, and φ_{vj} and φ'_{vj} are the driving amplitudes, frequencies, and phases, respectively. In experiments, the driving amplitudes $\{u_{vj}, u'_{vj}\}$ are of the order ~ 100 MHz, which are far larger than g_0. In such condition, when choosing $\Delta_{vj} = \omega_{vj}^0 - \omega_{v(j-1)}^0 = u_{vj}\,(-u_{vj})$ for odd (even) j, $\Delta_{ABj} = \omega_{Bj}^0 - \omega_{Aj}^0 = u'_{Bj}$, $\Delta_{BCj} = \omega_{Cj}^0 - \omega_{Bj}^0 = u'_{Cj}$, and $\Delta_{CAj} = \omega_{Aj}^0 - \omega_{Cj}^0 = u'_{Aj}$, we obtain an effective time-independent Hamiltonian (see Appendix A for details)

$$\hat{H} = \sum_{v,j}\left(t_{vj}e^{i\tilde{\varphi}_{vj}}\hat{a}^\dagger_{v(j-1)}\hat{a}_{vj} + \text{H.c.}\right) + \sum_{v\neq v',j}\tilde{t}_{vv'j}e^{i\tilde{\varphi}_{vv'j}}\hat{a}^\dagger_{vj}\hat{a}_{v'j}, \tag{18}$$

where the effective hopping strengths

$$t_{vj} = g_0 \mathrm{J}_0(\alpha_{v(j-1)})\mathrm{J}_1(\alpha_{vj})\mathrm{J}_0(\alpha'_{v(j-1)})\mathrm{J}_0(\alpha'_{vj}), \tag{19}$$

$$\tilde{t}_{vv'j} = g_0 \mathrm{J}_0(\alpha_{vj})\mathrm{J}_0(\alpha_{v'j})\mathrm{J}_0(\alpha'_{vj})\mathrm{J}_1(\alpha'_{v'j}), \tag{20}$$

with $\mathrm{J}_m(\cdot)$ indicating the m-th Bessel function of the first kind, $\alpha_{vj} = \varepsilon_{vj}/u_{vj}$, $\alpha'_{vj} = \varepsilon'_{vj}/u'_{vj}$, and the phases

$$\tilde{\varphi}_{vj} = (-1)^{j+1}\varphi_{vj} + \frac{\pi}{2}, \tag{21}$$

$$\tilde{\varphi}_{ABj} = -\tilde{\varphi}_{BAj} = \varphi'_{Bj} + \frac{\pi}{2}, \tag{22}$$

$$\tilde{\varphi}_{BCj} = -\tilde{\varphi}_{CBj} = \varphi'_{Cj} + \frac{\pi}{2}, \tag{23}$$

$$\tilde{\varphi}_{CAj} = -\tilde{\varphi}_{ACj} = \varphi'_{Aj} + \frac{\pi}{2}. \tag{24}$$

When choosing $\varphi'_{vj} = -\pi/2$, $\varphi_{Aj} = (-1)^{j+1}\varphi_0 - \pi/2$, $\varphi_{Bj} = 0$, and $\varphi_{Cj} = (-1)^j\varphi_0 - \pi/2$, we obtain an effective magnetic flux φ_0 in the $A_jA_{(j-1)}B_{(j-1)}B_j$ and $C_{(j-1)}C_jB_jB_{(j-1)}$ plaquettes and $2\varphi_0$ in the $A_jA_{(j-1)}C_{(j-1)}C_j$ plaquette, and thus realize a Hall tube governed by the Hamiltonian (18). Moreover, the corresponding parameters t_{vj} and $\tilde{t}_{vv'j}$ can be tuned independently by controlling the driving amplitudes and frequencies. For simplicity, in the following discussion, we apply a gauge transformation $\hat{b}_{vj} = \exp\{-\mathrm{i}[\varphi_0 j(s+1)]\}\hat{a}_{vj}$ ($s=-1,0,1$ for the legs A, B, and C) and choose the positive parameters with $t_{vj} = t_0$, $\tilde{t}_{ABj} = \tilde{t}_{BCj} = \tilde{t}$, and $\tilde{t}_{CAj} = t_{CA}$.

It should be emphasized that for the Hamiltonian (18), the boson operators satisfy the revised commutation relation $[\hat{a}_{vj}, \hat{a}^\dagger_{v',j'}] = (1-2\hat{n}_{vj})\delta_{v,v'}\delta_{j,j'}$ and meanwhile $\hat{a}^{\dagger 2}_{vj} = \hat{a}^2_{vj} = 0$. This means that the maximum occupation for each site is only one boson, which exhibits a hard-core boson property.[41–45] As a result, we call the Hall tube as the hard-core Hall tube. In the following, we consider the case of the single-qubit excitation.

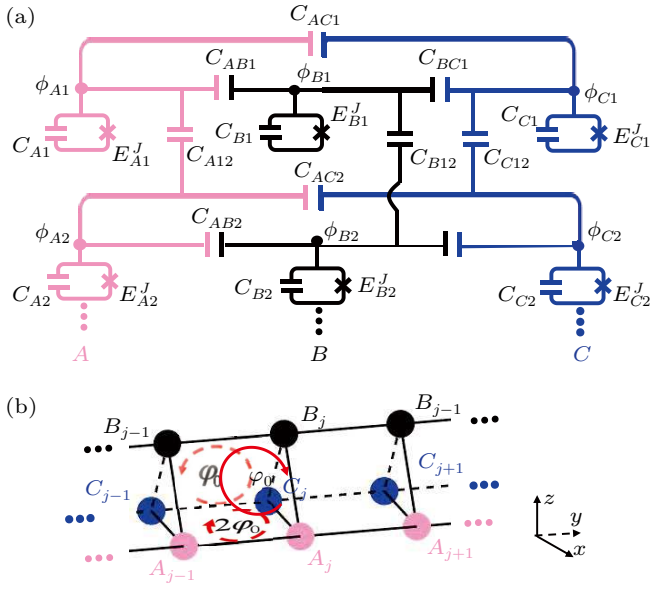


Fig. 1. (a) Three-leg (labeled respectively by A, B, and C) superconducting circuits with transmon qubits. Along each leg, the transmon qubits are coupled with their nearest-neighbor sites, while they interact with each other between legs at the same unit cell. All couplers are capacitors. C_{vj} and E^J_{vj} are the effective capacitance and the Josephson energy of the transmon qubit at the j-th site on the v-th leg. C_{vij} and $\{C_{ABj}, C_{BCj}, C_{CAj}\}$ are the capacitors to couple the transmon qubits at the j-th site on the v-th leg with its nearest-neighbor sites along each leg and between the legs, respectively. ϕ_{vj} is the node flux. (b) Schematics of the hard-core Hall tube with an effective magnetic flux φ_0 in the plaquettes $A_{(j-1)}A_jB_jB_{(j-1)}$ and $C_{(j-1)}C_jB_jB_{(j-1)}$ and $2\varphi_0$ in the plaquette $A_{(j-1)}A_jC_jC_{(j-1)}$. The pink, black, and blue filled circles indicate the transmon qubits in the A, B, and C legs, respectively.

3. Topological property

Having realized the tunable Hall tube, we now explore its fundamental property. We perform the Fourier transformation $\hat{b}_{vk} = (1/\sqrt{N})\sum_j e^{ikj}\hat{b}_{vj}$. As a result, the Hamiltonian (18) in the momentum space is given by $\hat{H} = \sum_k(\hat{b}^\dagger_{Ak}, \hat{b}^\dagger_{Bk}, \hat{b}^\dagger_{Ck})\hat{h}(k)(\hat{b}_{Ak}, \hat{b}_{Bk}, \hat{b}_{Ck})^{\mathrm{T}}$, where T is the transpose of matrix and

$$\hat{h}(k) = \begin{pmatrix} 2t_0\cos(\varphi_0-k) & \tilde{t} & t_{CA} \\ \tilde{t} & 2t_0\cos(k) & \tilde{t} \\ t_{CA} & \tilde{t} & 2t_0\cos(\varphi_0+k) \end{pmatrix}. \tag{25}$$

The eigenenergies of the Hamiltonian (25) are given by

$$E_1 = \sqrt[3]{-\frac{q}{2}+\sqrt{\Delta}} + \sqrt[3]{-\frac{q}{2}-\sqrt{\Delta}}, \tag{26}$$

$$E_2 = b_+\sqrt[3]{-\frac{q}{2}+\sqrt{\Delta}} + b_-\sqrt[3]{-\frac{q}{2}-\sqrt{\Delta}}, \tag{27}$$

$$E_3 = b_-\sqrt[3]{-\frac{q}{2}+\sqrt{\Delta}} + b_+\sqrt[3]{-\frac{q}{2}-\sqrt{\Delta}}, \tag{28}$$

where $b_\pm = (-1\pm\sqrt{3}\mathrm{i})/2$, $q = (2c_1^3 - 9c_1c_2 + 27c_3)/27$ with $c_1 = -2t_0[2\cos(\varphi_0)\cos(k)]$, $c_2 = 4t_0^2[2\cos(\varphi_0)\cos(k) + \cos(\varphi_0-k)\cos(\varphi_0+k)] - t_{CA}^2 - 2\tilde{t}^2$, and $c_3 = 2t_{CA}^2t_0\cos(k) + 4t_0\tilde{t}^2\cos(\varphi_0)\cos(k) - 8t_0^3\cos(\varphi_0-k)\cos(k)\cos(\varphi_0+k) + 2\tilde{t}^2t_{CA}$, and $\Delta = -(4p^3+27q^2)$ with $p = (3c_2 - c_1^2)/3$.

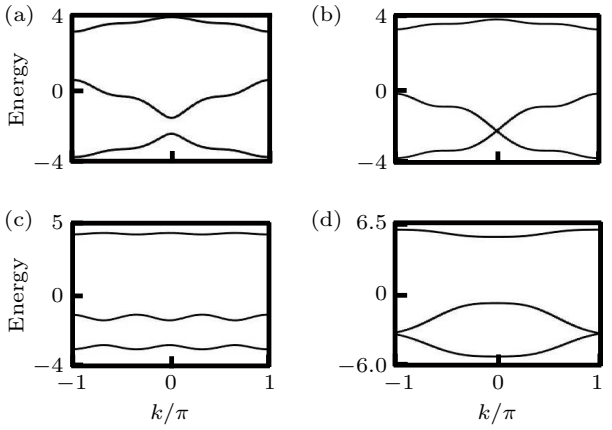


Fig. 2. Energy bands as functions of the momentum k with (a) $t_{CA} = 0.5$, (b) $t_{CA} = 1$, (c) $t_{CA} = 2$, and (d) $t_{CA} = 4$. The same parameters are $\varphi_0 = 2\pi/3$ and $\tilde{t} = 2$. Here t_0 is used as the unit.

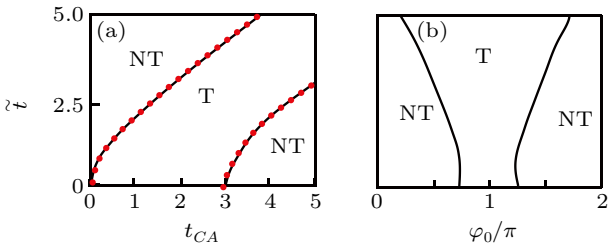


Fig. 3. Topological phase diagram in (a) t_{CA}–$\tilde{t}$ plane with $\varphi_0 = 2\pi/3$ and (b) φ_0–$\tilde{t}$ plane with $t_{CA} = 2$. T and NT indicate the topological nontrivial and trivial phases respectively. The black curves and red dots indicate the numerical and analytical results respectively. Here t_0 is used as the unit.

As shown by Eqs. (26)–(28), when t_{CA} is small, the energy bands is gapped [see Fig. 2(a)]. As t_{CA} increases to a critical value t^0_{CA}, the gapless energy bands occur at $k = 0$ [see Fig. 2(b)]. Further increasing t_{CA}, the bands gap reopens [see Fig. 2(c)]. Until t_{CA} increasing to another critical value t^π_{CA} shown in Fig. 2(d), the bands gap recloses at π. When $\Delta = 0$ and $\varphi_0 = 2\pi/3$, these critical points are obtained analytically by $t^0_{CA} = 1/2(-3t_0 + \sqrt{4\tilde{t}^2 + 9t_0^2})$ and $t^\pi_{CA} = 1/2(3t_0 + \sqrt{4\tilde{t}^2 + 9t_0^2})$. The gapless points always indicate phase boundaries that separate topological trivial and nontrivial phases.

Since the time–reversal, particle–hole, and chiral symmetries for the Hamiltonian (18) are all broken (see Appendix B for details), its topological property belongs to class A of the Altland–Zirnbauer classification.[46–49] The corresponding topological number is governed by the Zark phase defined as

$$Z_n = \int_{-\pi}^{\pi} \mathrm{d}k \, \langle u_n(k) | \, \partial_k \, | u_n(k) \rangle \,, \tag{29}$$

where $u_n(k)$ denotes the Bloch wavefunction of the n-th energy band. For $t_{CA} < t^0_{CA}$ and $t_{CA} > t^\pi_{CA}$, $Z_1 = Z_2 = 0$, while $Z_1 = Z_2 = 1$ for $t^0_{CA} \le t_{CA} \le t^\pi_{CA}$, which means that the first and second energy bands are topological nontrivial. Notice that for the whole regime, $Z_3 \equiv 0$, which shows that the topology of the third energy band is trivial. In Figs. 3(a) and 3(b), we obtain the phase diagram in t_{CA}–$\tilde{t}$ and φ_0–$\tilde{t}$ planes numerically respectively. The analytical phase boundaries t^0_{CA} and t^π_{CA} are denoted by the red solid points in Fig. 3(a).

3.1. Chiral edge currents

Chirality is a hallmark signature for the Hall effect. Based on the chirality, Meissner to vortex phase transition,[50–53] interaction-induced dynamical chiral currents,[54] chiral spin clusters,[55] photonic fractional topological insulators,[56–58] topological superfluid,[59–61] and superconductivity,[62] and moreover high-T_c superconductors[63,64] have been investigated. As a minimal model to simulate the integer Hall effect, the chirality of the Hall tube raises much interesting.

Since the Hall tube exhibits nontrivial topology, the chiral edge currents are expected to occur under the edge states.

In the topological nontrivial phase, the densities locate on the edges of the system. The interleg currents are defined as

$$\begin{aligned} \hat{J}_{ABj} &= \mathrm{i}\tilde{t}\hat{b}^\dagger_{Aj}\hat{b}_{Bj} + \mathrm{H.c.}, \\ \hat{J}_{BCj} &= \mathrm{i}\tilde{t}\hat{b}^\dagger_{Bj}\hat{b}_{Cj} + \mathrm{H.c.}, \\ \hat{J}_{CAj} &= \mathrm{i}t_{CA}\hat{b}^\dagger_{Cj}\hat{b}_{Aj} + \mathrm{H.c.} \end{aligned} \tag{30}$$

Under the edge state, these currents can be described as $J_{ABj} = \langle \hat{J}_{ABj} \rangle$, $J_{BCj} = \langle \hat{J}_{BCj} \rangle$, and $J_{CAj} = \langle \hat{J}_{CAj} \rangle$. The chiral edge currents are characterized by nonzero J_{AB1}, J_{BC1}, and J_{CA1} (J_{ABN}, J_{BCN}, and J_{CAN}) with the same sign.

To see the chiral edge currents, we plot the currents and densities distributions in Figs. 4(a) and 4(b) with $\tilde{t} = t_{CA} = 2$ under the L-th and $(L+1)$-th eigen states of the Hamiltonian (18) respectively. It is obviously, the currents located on the edges of the tube have chirality. Moreover the currents under different states have opposite directions, which corresponds with the integer quantum Hall effects in two dimensional system. By numerical calculation, we find J_{AB1} (J_{BC1}) and J_{BCN} (J_{ACN}) are always equal, which is also shown in Figs. 4(c) and 4(d). In Figs. 4(c)–4(f) we plot the phase diagrams as functions of $\tilde{t}$ and t_{CA}. We can see when $\tilde{t} = t_{CA}$, J_{AB1}, J_{BC1}, and J_{CA1} become nonzero(zero) with J_{ABN}, J_{BCN}, and J_{CAN} become zero (nonzero) respectively, which means the chiral currents only locate on one edge. When $\tilde{t} \neq t_{CA}$, J_{AB1}, J_{BC1}, and J_{CA1} always have opposite values with J_{ABN}, J_{BCN}, and J_{CAN} respectively, which indicates the chiral currents have opposite direction between the edges with $j = 1$ and $j = N$. Moreover, the chiral edge currents are found in the topological nontrivial phase indicated by TC in Fig. 4(g).

In the practical experiments, the exact values of the coupling strength can not be tuned. Considering the influence of the imperfections in device fabrication, the imperfection Hamiltonian can be written as

$$\delta\hat{H} = \sum_j \delta t_{Aj} \mathrm{e}^{\mathrm{i}\varphi_0} \hat{b}^\dagger_{Aj}\hat{b}_{A(j+1)} + \delta t_{Bj}\hat{b}^\dagger_{Bj}\hat{b}_{B(j+1)}$$

$$+\delta t_{Cj}\mathrm{e}^{-\mathrm{i}\varphi_0}\hat{b}^{\dagger}_{Cj}\hat{b}_{C(j+1)}+\delta t_{ABj}\hat{b}^{\dagger}_{Aj}\hat{b}_{Bj}$$
$$+\delta t_{BCj}\hat{b}^{\dagger}_{Bj}\hat{b}_{Cj}+\delta t_{CAj}\hat{b}^{\dagger}_{Cj}\hat{b}_{Aj}+\mathrm{H.c.}, \quad (31)$$

where δt_{vj} and $\delta t_{vv'j}$ equal to $W\delta$. W is the imperfection strength and $\delta\in[-0.5,0.5]$ is a random number. The corresponding imperfection chiral edge currents also with the imperfection hopping strength. We show the imperfection influence of the chiral currents in Fig. 4(h). We plot the total edge currents $J_{\mathrm{E}}=|J_{AB1}|+|J_{BC1}|+|J_{CA1}|+|J_{ABN}|+|J_{BCN}|+|J_{CAN}|$ as a function of $\log_{10}W$ with $\tilde{t}=t_{CA}=2$. As $\log_{10}W$ increasing, J_{E} decreases slowly in the case of $\log_{10}W<-1$. When $\log_{10}W>-1$, J_{E} suddenly decreases with $\log_{10}W$ increasing. This means when the strength of the imperfection is not large enough, the chiral edge currents are robust.

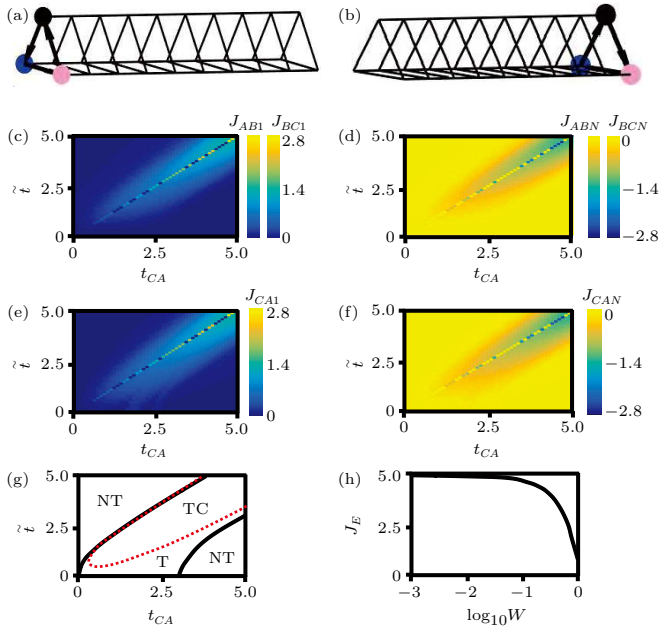


Fig. 4. Chiral edge currents and densities distributions on the Hall tube with $\tilde{t}=t_{CA}=2$ under (a) the L-th and (b) $(L+1)$-th edge states. The thicknesses of the arrows indicate their strengths. The pink, black, and blue filled circles denote the local densities on legs A, B, and C respectively. Phase diagram of (c) J_{AB1} and J_{BC1}, (d) J_{ABN} and J_{BCN}, (e) J_{CA1}, and (f) J_{CAN} as functions of t_{CA} and $\tilde{t}$. (g) Chiral edge currents phase emerging in the topological nontrival phase is indicated by TC. (h) J_{E} as the function of $\log_{10}W$ with $\tilde{t}=t_{CA}=2$. The same parameter is $\varphi_0=2/3\pi$. Here t_0 is used as the unit.

4. Possible experimental observation

In theoretical analysis, for showing the physical phenomena clearly we need consider large size and large parameters interval. While in experiments, to obtain the topological state [Figs. 5(a) and 5(b)] and the corresponding chiral edge currents [Figs. 5(c) and 5(d)] we just need four unit cells and a group fixed parameters. For simplicity we choose the parameters as $\tilde{t}=t_{CA}=t_0$. In this case, we just need single alternating-current microwave to drive each qubit, because when $\varepsilon'_{vj}=0$, $a_{vj}=\alpha$, $\Delta_{vj}=u_{vj}$ $(-u_{vj})$, $\Delta_{ABj}=u_{Bj}$ $(-u_{Bj})$, $\Delta_{BCj}=u_{Cj}$ $(-u_{Cj})$, and $\Delta_{CAj}=u_{Aj}$ $(-u_{Aj})$ for odd (even) j, all coupling strengths reduce as $g_0\mathrm{J}_0(\alpha)\mathrm{J}_1(\alpha)$. For obtaining gauge-invariant magnetic flux φ_0, the phases should be set as $\tilde{\varphi}_{vj}=(-1)^{j+1}\varphi_{vj}+\pi/2$, $\tilde{\varphi}_{ABj}=-\tilde{\varphi}_{BAj}=(-1)^{j+1}\varphi_{Bj}+\pi/2$, $\tilde{\varphi}_{BCj}=-\tilde{\varphi}_{CBj}=(-1)^{j+1}\varphi_{Cj}+\pi/2$, and $\tilde{\varphi}_{CAj}=-\tilde{\varphi}_{ACj}=(-1)^{j+1}\varphi_{Aj}+\pi/2$ with considering $\varphi_{vj}=(-1)^{j+1}\varphi_0 j-\pi/2$.

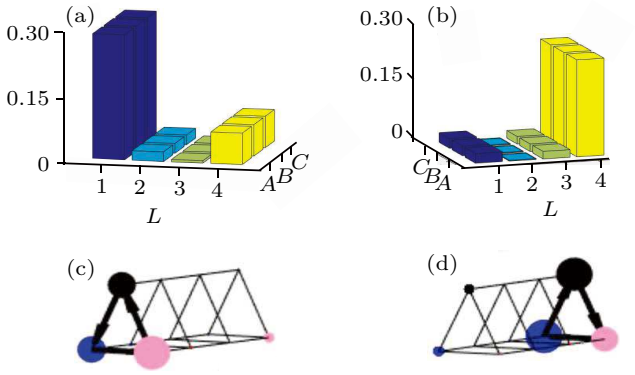


Fig. 5. Densities distributions of the edge states with (a) the L-th and (b) the $(L+1)$-th wavefunctions. The corresponding chiral edge currents and densities distributions on the Hall tube are shown in panels (c) and (d). The thicknesses of the arrows indicate their strengths. The pink, black, and blue filled circles denote the local densities on legs A, B, and C respectively. The parameters are $\tilde{t}=t_{CA}=1$, $\varphi_0=2/3\pi$, and $L=4$. Here t_0 is used as the unit.

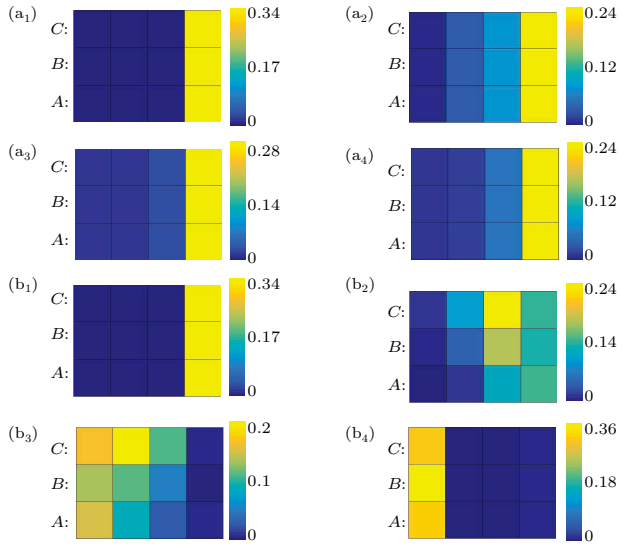


Fig. 6. Densities distributions at each site with the initial state $(\hat{a}^{\dagger}_{A1}+\hat{a}^{\dagger}_{B1}+\hat{a}^{\dagger}_{C1})/\sqrt{3}\,|0\rangle$ with (a_1) and (b_1) $t=0$ ns, (a_2) and (b_2) $t=100$ ns, (a_3) and (b_3) $t=200$ ns, and (a_4) and (b_4) $t=300$ ns. $\varphi_0=2/3\pi$ and 0.1π for (a_1)–(a_4) and (b_1)–(b_4) respectively. The common parameters are $\tilde{t}=t_{CA}=1$. Here t_0 is used as the unit.

To prepare the edge state $|\psi\rangle_{\mathrm{E}}=(\hat{b}^{\dagger}_{AL}+\hat{b}^{\dagger}_{BL}+\hat{b}^{\dagger}_{CL})\,|0\rangle/\sqrt{3}$ [Fig. 5(b)], we first turn off all couplings between any qubits. Then we excite one qubit at arbitrary site with $j=L$ and turn on the coupling strength $\tilde{t}$ and t_{CA}, allowing this excitation to swap to the other two qubits at the end of the tube.[65] In Fig. 6, we show the dynamics in the topological non-trivial [Figs. 6(a_1)–6(a_4)] and trivial [Figs. 6(b_1)–6(b_4)] phases with the prepared initial state $|\psi\rangle_{\mathrm{E}}$. We can see the densities in the topological non-trivial and trivial phases are located and dispersed respectively. After preparing the edge

state $|\psi\rangle_{\rm E}$, the corresponding density matrix $\hat{\rho}_{\rm E}$ can be constructed by quantum state tomography.[66,67] This means that the chiral edge currents can be obtained by $\mathrm{tr}(\hat{\rho}_{\rm E}\hat{J}_{\nu\nu' j})$ with $j=1$ or 4.[65]

5. Conclusion

In summary, we proposed a feasible experiment scheme using three legs superconducting circuits with transmon qubits to realize a hard-core Hall tube. Then we first investigate its topological properties. Since the time–reversal, particle–hole, and chiral symmetries are all broken for the hard-core Hall tube, it belongs to the A class of the Altland–Zirnbauer classification. We obtain the corresponding topological phase transition both numerically and analytically. The chirality is a key character of the quantum Hall effect, thus we secondly investigate the chiral physics in the hard-core Hall tube. In the topological nontrival phase, we find the topological protected chiral edge currents and discuss its robustness with imperfection influence. Finally, we give the possible experimental observations of the topological state and topological protected chiral edge currents in the hard-core Hall tube.

Appendix A: Derivation of the effective Hamiltonian (18)

For obtaining the Hamiltonian (18), we apply the rotation frame with the following unitary operator

$$\hat{U}=\hat{U}_1\times\hat{U}_2\times\hat{U}_3, \tag{A1}$$

where

$$\hat{U}_1 = \exp\left[-\mathrm{i}\sum_{j=1}^{N}\sum_{\nu}\omega_{\nu j}^{0}\hat{a}_{\nu j}^{\dagger}\hat{a}_{\nu j}t\right], \tag{A2}$$

$$\hat{U}_2 = \exp\left[\mathrm{i}\sum_{j=1}^{N}\sum_{\nu}\alpha_{\nu j}\hat{a}_{\nu j}^{\dagger}\hat{a}_{\nu j}\cos\left(u_{\nu j}t+\varphi_{\nu j}\right)\right], \tag{A3}$$

$$\hat{U}_3 = \exp\left[\mathrm{i}\sum_{j=1}^{N}\sum_{\nu}\alpha_{\nu j}'\hat{a}_{\nu j}^{\dagger}\hat{a}_{\nu j}\cos\left(u_{\nu j}'t+\varphi_{\nu j}'\right)\right], \tag{A4}$$

with $\alpha_{\nu j}=\varepsilon_{\nu j}/u_{\nu j}$ and $\alpha_{\nu j}'=\varepsilon_{\nu j}'/u_{\nu j}'$, the Hamiltonian with the time-dependent frequency $\omega_{\nu j}(t)$ is transformed as

$$\hat{H}=\hat{U}^{\dagger}\hat{H}\hat{U}+\mathrm{i}\frac{\mathrm{d}\hat{U}^{\dagger}}{\mathrm{d}t}\hat{U}=\hat{H}_{\rm E}+\hat{H}_{\rm I}, \tag{A5}$$

where

$$\begin{aligned}\hat{H}_{\rm E} = &\sum_{\nu}g_0\left\{\hat{a}_{\nu 1}^{\dagger}\hat{a}_{\nu 2}\exp(-\mathrm{i}\Delta_{\nu 2}t)\exp\left[-\mathrm{i}\alpha_{\nu 1}\cos\left(u_{\nu 1}t+\varphi_{\nu 1}\right)\right]\exp\left[\mathrm{i}\alpha_{\nu 2}\cos\left(u_{\nu 2}t+\varphi_{\nu 2}\right)\right]\right.\\
&\left.\times\exp\left[-\mathrm{i}\alpha_{\nu 1}'\cos\left(u_{\nu 1}'t+\varphi_{\nu 1}'\right)\right]\exp\left[\mathrm{i}\alpha_{\nu 2}'\cos\left(u_{\nu 2}'t+\varphi_{\nu 2}'\right)\right]+\mathrm{H.c.}\right\}\\
&+g_0\left\{\hat{a}_{\nu 2}^{\dagger}\hat{a}_{\nu 3}\exp(-\mathrm{i}\Delta_{\nu 3}t)\exp\left[-\mathrm{i}\alpha_{\nu 2}\cos\left(u_{\nu 2}t+\varphi_{\nu 2}\right)\right]\exp\left[\mathrm{i}\alpha_{\nu 3}\cos\left(u_{\nu 3}t+\varphi_{\nu 3}\right)\right]\right.\\
&\left.\times\exp\left[-\mathrm{i}\alpha_{\nu 2}'\cos\left(u_{\nu 2}'t+\varphi_{\nu 2}'\right)\right]\exp\left[\mathrm{i}\alpha_{\nu 3}'\cos\left(u_{\nu 3}'t+\varphi_{\nu 3}'\right)\right]+\mathrm{H.c.}\right\}+\cdots,\end{aligned} \tag{A6}$$

$$\begin{aligned}\hat{H}_{\rm I} = &\sum_{\nu\neq\nu'}g_0\left\{\hat{a}_{\nu 1}^{\dagger}\hat{a}_{\nu' 2}\exp(-\mathrm{i}\Delta_{\nu\nu' 1}t)\exp\left[-\mathrm{i}\alpha_{\nu 1}\cos\left(u_{\nu 1}t+\varphi_{\nu 1}\right)\right]\exp\left[\mathrm{i}\alpha_{\nu' 1}\cos\left(u_{\nu' 1}t+\varphi_{\nu' 1}\right)\right]\right.\\
&\left.\times\exp\left[-\mathrm{i}\alpha_{\nu 1}'\cos\left(u_{\nu 1}'t+\varphi_{\nu 1}'\right)\right]\exp\left[\mathrm{i}\alpha_{\nu' 1}'\cos\left(u_{\nu' 1}'t+\varphi_{\nu' 1}'\right)\right]+\mathrm{H.c.}\right\}\\
&+g_0\left\{\hat{a}_{\nu 2}^{\dagger}\hat{a}_{\nu' 2}\exp(-\mathrm{i}\Delta_{\nu\nu' 2}t)\exp\left[-\mathrm{i}\alpha_{\nu 2}\cos\left(u_{\nu 2}t+\varphi_{\nu 2}\right)\right]\exp\left[\mathrm{i}\alpha_{\nu' 2}\cos\left(u_{\nu' 2}t+\varphi_{\nu' 2}\right)\right]\right.\\
&\left.\times\exp\left[-\mathrm{i}\alpha_{\nu 2}'\cos\left(u_{\nu 2}'t+\varphi_{\nu 2}'\right)\right]\exp\left[\mathrm{i}\alpha_{\nu' 2}'\cos\left(u_{\nu' 2}'t+\varphi_{\nu' 2}'\right)\right]+\mathrm{H.c.}\right\}+\cdots,\end{aligned} \tag{A7}$$

where $\Delta_{\nu j}=\omega_{\nu j}^{0}-\omega_{\nu(j-1)}^{0}$ and $\Delta_{\nu\nu' j}=\omega_{\nu' j}^{0}-\omega_{\nu j}^{0}$. Using the Jacobi–Anger identity,

$$\exp\left[\mathrm{i}\alpha\cos\left(ut+\varphi\right)\right]=\sum_{-\infty}^{\infty}\mathrm{i}^{m}\mathrm{J}_m(\alpha)\exp\left[\mathrm{i}m\left(ut+\varphi\right)\right],$$

we have

$$\begin{aligned}\hat{H}_{\rm E} = &\sum_{\nu,j}g_0\hat{a}_{\nu(j-1)}^{\dagger}\hat{a}_{\nu j}\sum_{m_1=-\infty}^{\infty}(-\mathrm{i})^{m_1}\mathrm{J}_{m_1}\left(\alpha_{\nu(j-1)}\exp\left[-\mathrm{i}m_1\left(u_{\nu(j-1)}t+\varphi_{\nu(j-1)}\right)\right]\right.\\
&\times\sum_{m_2=-\infty}^{\infty}\mathrm{i}^{m_2}\mathrm{J}_{m_2}(\alpha_{\nu j})\exp\left[\mathrm{i}\left(m_2u_{\nu j}-\Delta_{\nu j}\right)t+m_2\varphi_{\nu j}\right]\\
&\times\sum_{m_3=-\infty}^{\infty}(-\mathrm{i})^{m_3}\mathrm{J}_{m_3}(\alpha_{\nu(j-1)}')\exp\left[-\mathrm{i}m_3\left(u_{\nu(j-1)}'t+\varphi_{\nu(j-1)}'\right)\right]\\
&\times\sum_{m_4=-\infty}^{\infty}\mathrm{i}^{m_4}\mathrm{J}_{m_4}(\alpha_{\nu j}')\exp\left[\mathrm{i}m_4\left(u_{\nu j}'t+\varphi_{\nu j}'\right)\right]+\mathrm{H.c.},\end{aligned} \tag{A8}$$

$$\begin{aligned}\hat{H}_{\rm I} = & \sum_{\nu\neq\nu',j} g_0\hat{a}^{\dagger}_{\nu j}\hat{a}_{\nu' j}\sum_{m_1=-\infty}^{\infty}(-{\rm i})^{m_1}{\rm J}_{m_1}(\alpha_{\nu j})\exp\left[-{\rm i}m_1\left(u_{\nu j}t+\varphi_{\nu j}\right)\right]\\ & \times\sum_{m_2=-\infty}^{\infty}{\rm i}^{m_2}{\rm J}_{m_2}(\alpha_{\nu' j})\exp\left[{\rm i}m_2\left(u_{\nu' j}t+\varphi_{\nu' j}\right)\right]\\ & \times\sum_{m_3=-\infty}^{\infty}(-{\rm i})^{m_3}{\rm J}_{m_3}(\alpha'_{\nu j})\exp\left[-{\rm i}m_3\left(u'_{\nu j}t+\varphi'_{\nu j}\right)\right]\\ & \times\sum_{m_4=-\infty}^{\infty}{\rm i}^{m_4}{\rm J}_{m_4}(\alpha'_{\nu' j})\exp\left[{\rm i}\left(m_4u'_{\nu' j}-\Delta_{\nu\nu' j}\right)t+m_4\varphi'_{\nu' j}\right]+{\rm H.c.}\end{aligned}\tag{A9}$$

When choosing $\Delta_{\nu j}=u_{\nu j}$ $(-u_{\nu j})$ for odd (even) j, $\Delta_{ABj}=u'_{Bj}$, $\Delta_{BCj}=u'_{Cj}$, and $\Delta_{CAj}=u'_{Aj}$, considering the case that $\left\{u_{\nu j},u'_{\nu j}\right\}\gg g_0$, the oscillating terms in the Hamiltonians (A8) and (A9) are neglected by applying the rotating-wave approximation. As a result, the effective Hamiltonian (18) with parameters in Eqs. (19)–(24) is derived.

Appendix B: Symmetries for the Hall tube

The time-reversal operator $\hat{\mathcal{T}}$, particle-hole operator $\hat{\mathcal{C}}$ and chiral operator $\hat{\mathcal{S}}$ generally transform the bosonic operators as $\hat{\mathcal{T}}\hat{b}_{\nu j}\hat{\mathcal{T}}^{-1}=\hat{b}_{\nu j}$, $\hat{\mathcal{C}}\hat{b}_{\nu j}\hat{\mathcal{C}}^{-1}=(-1)^i\hat{b}^{\dagger}_{\nu j}$, and $\hat{\mathcal{S}}\hat{b}_{\nu j}\hat{\mathcal{S}}^{-1}=(-1)^i\hat{b}^{\dagger}_{\nu j}$, respectively, and moreover, $\hat{\mathcal{T}}i\hat{\mathcal{T}}^{-1}=\hat{\mathcal{S}}i\hat{\mathcal{S}}^{-1}=-i$. Since the Hamiltonian (18) is changed under any of these transformation, the time-reversal, particle-hole, and chiral symmetries are all broken. Moreover, the protecting symmetry for the Hamiltonian (18) is an inversion symmetry and the corresponding operator $\hat{\mathcal{I}}$ transform the bosonic operator as $\hat{\mathcal{I}}\hat{b}_{\nu j}\hat{\mathcal{I}}^{-1}=\hat{M}_{\nu,\nu'}\hat{b}_{\nu'(-j)}$. $\hat{M}$ is a unitary matrix act on the legs of the Hall tube. When choosing $\hat{M}$ as a matrix with the antidiagonal elements as 1 and the other elements as zero, the Hamiltonian (18) under the transformations $\hat{\mathcal{I}}\hat{b}_{Aj}\hat{\mathcal{I}}^{-1}=\hat{b}_{C(-j)}$, $\hat{\mathcal{I}}\hat{b}_{Bj}\hat{\mathcal{I}}^{-1}=\hat{b}_{B(-j)}$, and $\hat{\mathcal{I}}\hat{b}_{Cj}\hat{\mathcal{I}}^{-1}=\hat{b}_{A(-j)}$ is unchanged. It needs to be emphasized that when the inversion symmetry is broken, the topological nontrivial will disappear.[68]

Acknowledgments

Project supported by the National Key Program of the National Health Commission's "Thirteenth Five-Year Plan" (Grant No. NHFPC102018), the Ministry of Education Collaborative Education Program (Grant No. 202101029006), the Natural Science Foundation of Shanxi Province, China (Grant No. 202103021223010), the Shanxi Province Higher Education Science and Technology Innovation Program (Grant No. J2021770), and the Natural Science Foundation of Taiyuan University, China (Grant No. 21TYKQ22).

References

[1] Hasan M Z and Kane C L 2010 *Rev. Mod. Phys.* **82** 3045
[2] Moore J 2010 *Nature* **464** 194
[3] Qi X L and Zhang S C 2011 *Rev. Mod. Phys.* **83** 1057
[4] Tokura Y, Yasuda K and Tsukazaki A 2019 *Nat. Rev. Phys.* **1** 126
[5] Klitzing K V, Dorda G and Pepper M 1980 *Phys. Rev. Lett.* **45** 494
[6] Senthil T and Levin M 2013 *Phys. Rev. Lett.* **110** 046801
[7] Xu Y, Miotkowski I, Liu C, Tian J, Nam H, Alidoust N, Hu J, Shih C K, Hasan M Z and Chen Y P 2014 *Nat. Phys.* **10** 956
[8] Kozlovsky R, Graf A, Kochan D, Richter K and Gorini C 2020 *Phys. Rev. Lett.* **124** 126804
[9] Klitzing K, Chakraborty T, Kim P, Madhavan V, Dai X, McIver J, Tokura Y, Savary L, Smirnova D, Rey A M, Felser C, Gooth J and Qi X 2020 *Nat. Rev. Phys.* **2** 397
[10] Hofstadter D R 1976 *Phys. Rev. B* **14** 2239
[11] Dean C R, Wang L, Maher P, Forsythe C, Ghahari F, Gao Y, Katoch J, Ishigami M, Moon P, Koshino M, Taniguchi T, Watanabe K, Shepard K L, Hone J and Kim P 2013 *Nature* **497** 598
[12] Aidelsburger M, Atala M, Lohse M, Barreiro J T, Paredes B and Bloch I 2013 *Phys. Rev. Lett.* **111** 185301
[13] Miyake H, Siviloglou G A, Kennedy C J, Burton W C and Ketterle W 2013 *Phys. Rev. Lett.* **111** 185302
[14] Aidelsburger M, Lohse M, Schweizer C, Atala M, Barreiro J T, Nascimbéne S, Cooper N R, Bloch I and Goldman N 2015 *Nat. Phys.* **11** 162
[15] Stuhl B K, Lu H I, Aycock L M, Genkina D and Spielman I B 2015 *Science* **349** 1514
[16] Mancini M, Pagano G, Cappellini G, Livi L, Rider M, Catani J, Sias C, Zoller P, Inguscio M, Dalmonte M and Fallani L 2015 *Science* **349** 1510
[17] Han J H, Kang J H and Shin Y 2019 *Phys. Rev. Lett.* **122** 065303
[18] Xiang Z L, Ashhab S, You J Q and Nori F 2013 *Rev. Mod. Phys.* **85** 623
[19] Gu X, Kockum A F, Miranowicz A, Liu Y and Nori F 2017 *Phys. Rep.* **718–719** 1
[20] Buluta I, Ashhab S and Nori F 2011 *Rep. Prog. Phys.* **74** 104401
[21] Arute F, Arya K, Babbush R, Bacon D, Bardin J C, Barends R, Biswas R, Boixo S, Brandao F G S L, Buell D A, *et al.* 2019 *Nature* **574** 505
[22] Wendin G 2017 *Rep. Phys.* **80** 106001
[23] Blais A, Girvin S M and Oliver W D 2020 *Nat. Phys.* **16** 247
[24] Houck A A, Türeci H E and Koch J 2012 *Nat. Phys.* **8** 292
[25] Schmidt S and Koch J 2013 *Ann. Phys.* **525** 395
[26] Georgescu I M, Ashhab S and Nori F 2014 *Rev. Mod. Phys.* **86** 153
[27] Kyriienko O and Srensen A S 2018 *Phys. Rev. Appl.* **9** 064029
[28] Schroer M D, Kolodrubetz M H, Kindel W F, Sandberg M, Gao J, Vissers M R, Pappas D P, Polkovnikov A and Lehnert K W 2014 *Phys. Rev. Lett.* **113** 050402
[29] Roushan P, Neill C, Chen Y, Kolodrubetz M, *et al.* 2014 *Nature* **515** 241
[30] Wang T, Zhang Z, Xiang L, Gong Z, Wu J and Yin Y 2018 *Sci. China-Phys. Mech. Astron.* **61** 047411
[31] Tan X, Zhang D W, Liu Q, Xue G, Yu H F, Zhu Y Q, Yan H, Zhu S L and Yu Y 2018 *Phys. Rev. Lett.* **120** 130503
[32] Ramasesh V V, Flurin E, Rudner M, Siddiqi I and Yao N Y 2017 *Phys. Rev. Lett.* **118** 130501
[33] Flurin E, Ramasesh V V, Hacohen G S, Martin L S, Yao N Y and Siddiqi I 2017 *Phys. Rev. X* **7** 031023
[34] Cai W, Han J, Mei F, Xu Y, Ma Y, Li X, Wang H, Song Y P, Xue Z Y, Yin Z Q, *et al.* 2019 *Phys. Rev. Lett.* **123** 080501
[35] Li X, Cai T, Yan H, Wang Z, Pan X, Ma Y, Cai W, Han J, Hua Z, Han X, Wu Y, Zhang H, Wang H, Song Y, Duan L and Sun L 2020 *Phys. Rev. Appl.* **14** 024070

[36] Han X. Y, Cai T Q, Li X G, Wu Y K, Ma Y W, Ma Y L, Wang J H, Zhang H Y, Song Y P and Duan L M 2020 *Phys. Rev. A* **102** 022619

[37] Koch J, Yu T M, Gambetta J, Houck A A, Schuster D I, Majer J, Blais A, Devoret M H, Girvin S M and Schoelkopf R J 2007 *Phys. Rev. A* **76** 042319

[38] Caldwell S, Didier N, Ryan C A, Sete E A, Hudson A, Karalekas P, Manenti R, da Silva M P, Sinclair R and Acala E 2018 *Phys. Rev. Appl.* **10** 034050

[39] Li X, Ma Y, Han J, Chen T, Xu Y, Cai W, Wang H, Song Y P, Xue Z Y, Yin Z Q and Sun L 2018 *Phys. Rev. Appl.* **10** 054009

[40] Reagor M, Osborn C B, Tezak N, Staley A, Prawiroatmodjo G, Scheer M, Alidoust N, Sete E A, Didier N and da Silva M P 2018 *Sci. Adv.* **4** eaao3603

[41] Girardeau M 1960 *J. Math. Phys.* **1** 516

[42] Rigol M and Muramatsu A 2005 *Phys. Rev. A* **72** 013604

[43] Vidmar L, Ronzheimer J P, Schreiber M, Braun S, Hodgman S S, Langer S, Meisner F H, Bloch I and Schneider U 2015 *Phys. Rev. Lett.* **115** 175301

[44] Ardila L A P, Hey M and Eckardt A 2018 *Phys. Rev. Lett.* **121** 260401

[45] Yanay Y, Braumüller J, Gustavsson S and Oliver W D 2020 *npj Quantum Inf.* **6** 58

[46] Altland A and Zirnbauer M R 1997 *Phys. Rev. B* **55** 1142

[47] Schnyder A P, Ryu S, Furusaki A and Ludwig A W W 2008 *Phys. Rev. B* **78** 195125

[48] Ludwig A W W 2016 *Phys. Scr. T.* **T168** 014001

[49] Chiu C K, Teo J C Y, Schnyder A P and Ryu S 2016 *Rev. Mod. Phys.* **88** 035005

[50] Atala M, Aidelsburger M, Lohse M, Barreiro J T, Paredes B and Bloch I 2014 *Nat. Phys.* **10** 588

[51] Piraud M, Meisner F H, McCulloch I P, Greschner S, Vekua T and Schollwöck U 2015 *Phys. Rev. B* **91** 140406

[52] Sachdeva R, Metz F, Singh M, Mishra T and Busch T 2018 *Phys. Rev. A* **98** 063612

[53] Guan X, Feng Y, Xue Z Y, Chen G and Jia S 2020 *Phys. Rev. A* **102** 032610

[54] Tai M E, Lukin A, Rispoli M, Schittko R, Menke T, Borgnia D, Preiss P M, Grusdt F, Kaufman A M and Greiner M 2017 *Nature* **546** 519

[55] Wang D W, Song C, Feng W, Cai H, Xu D, Deng H, Li H K, Zheng D N, Zhu X B, Wang H, Zhu S Y and Scully M O 2019 *Nat. Phys.* **15** 382

[56] Levin M and Stern A 2009 *Phys. Rev. Lett.* **103** 196803

[57] Klinovaja J, Yacoby A and Loss D 2014 *Phys. Rev. B* **90** 155447

[58] Santos R A, Huang C W, Gefen Y and Gutman D B 2015 *Phys. Rev. B* **91** 205141

[59] Levitin L V, Bennett R G, Casey A, Cowan B, Saunders J, Drung D, Schurig T and Parpia J M 2013 *Science* **340** 841

[60] Autti S, Dmitriev V V, Mäkinen J T, Soldatov A A, Volovik G E, Yudin A N, Zavjalov V V and Eltsov V B 2016 *Phys. Rev. Lett.* **117** 255301

[61] Jia W, Huang Z H, Wei X, Zhao Q and Liu X J 2019 *Phys. Rev. B* **99** 094520

[62] Jiang Y F and Jiang H C 2020 *Phys. Rev. Lett.* **125** 157002

[63] Fauqué B, Sidis Y, Hinkov V, Pailhès S, Lin C T, Chaud X and Bourges P 2006 *Phys. Rev. Lett.* **96** 197001

[64] Morenzoni E, Wojek B M, Suter A, Prokscha T, Logvenov G and Božović I 2011 *Nat. Commun.* **2** 272

[65] Roushan P, Neill C, Megrant A, Chen Y, Babbush R, Barends R, Campbell B, Chen Z, Chiaro B, Dunsworth A, Fowler A, Jeffrey E, Kelly J, Lucero E, Mutus J, O'Malley P J J, Neeley M, Quintana C, Sank D, Vainsencher A, Wenner J, White T, Kapit E, Neven H and Martinis J 2017 *Nat. Phys.* **13** 146

[66] Steffen M, Ansmann M, McDermott R, Katz N, Bialczak R C, Lucero E, Neeley M, Weig E M, Cleland A N and Martinis J M 2006 *Phys. Rev. Lett.* **97** 050502

[67] Song C, Xu K, Liu W, Yang C P, Zheng S B, Deng H, Xie Q, Huang K, Guo Q, Zhang L, Zhang P, Xu D, Zheng D, Zhu X, Wang H, Chen Y A, Lu C Y, Han S and Pan J W 2017 *Phys. Rev. Lett.* **119** 180511

[68] Barbarino S, Dalmonte M, Fazio R and Santoro G E 2018 *Phys. Rev. A* **97** 013634